Melt processing of paramylon using a water:ionic liquid mixture as plasticizer

Frédérica Feuzing, Jean Pierre Mbakidi, Bruno Pontoire, Delphine Quéveau, Guillaume Roelens, Denis Lourdin, Sandrine Bouquillon, Eric Leroy

Accepted manuscript published in the journal Carbohydrate Polymers
https://doi.org/10.1016/j.carbpol.2023.120607

Melt processing of paramylon using a water:ionic liquid mixture as plasticizer

Frédérica Feuzing,[a,b] Jean Pierre Mbakidi,[b] Bruno Pontoire,[c], Delphine Quéveau[a], Guillaume Roelens[a], Denis Lourdin,[c] Sandrine Bouquillon,[b] & Eric Leroy,[a,*]

[a] Université de Nantes, Oniris, CNRS, GEPEA, UMR 6144, F- 44470 Carquefou, France.

[b] Institut de Chimie Moléculaire de Reims, CNRS UMR 7312, Université de Reims Champagne-Ardenne, BP 1039, 51687 Reims Cedex, France
[c] Biopolymers Interactions Assemblies Research Unit 1268 (BIA), INRAE, Rue de la Géraudière, 44316, Nantes, France

* Corresponding author: eric.leroy@univ-nantes.fr

Abstract

Paramylon is a linear β-1,3-glucan produced by the microalgae *Euglena Gracilis*. Due to its native crystalline structure, involving hexagonally packed triple helices, paramylon is neither water soluble nor thermoplastic. While such properties are generally obtained by chemical modification of paramylon, the present work demonstrates that using ionic liquid/water mixtures as solvents or plasticizers may be an alternative: A mixture of water with cholinium glycinate (40:60) allowed: i) obtaining paramylon solutions at 80°C, that form reversible ionogels upon cooling at 20°C, when used as a solvent, and ii) the thermomechanical processing of paramylon below 100°C by extrusion and hot-press into transparent films, when used as a plasticizer. The thermoplastic paramylon obtained consists of an amorphous matrix, self-reinforced by oriented triple helices packed as nanofibers. This results in a storage modulus ranging from 300 to 450 MPa at 25°C, depending on the plasticizer content, and in a tensile strain at break of 27%. For storage times larger than 1 month, a recrystallization of paramylon is observed, with an unidentified crystalline structure different from the native one. Recrystallised samples can be reprocessed into amorphous films by hot pressing.

Keywords: β-1,3- glucan, ionic liquid, plasticizer, melt processing, microalgae

1) Introduction

Paramylon is a linear β-1,3-glucan, produced by an industrially cultivable microalga (*Euglena gracilis*). Despite its promising bioactive and mechanical properties, the processing routes to make materials based on this polysaccharide without chemical modification are limited by its low solubility and absence of thermoplasticity, as discussed in detail in a recent review (Feuzing et al., 2022). Indeed, during its biosynthesis as intracellular granules, paramylon chains take a triple helix conformation stabilized by hydrogen bonds (Chuah et al., 1983). These triple helix takes part in the formation of a highly stable hexagonal crystalline structure (Marchessault & Deslandes, 1979), leading to nanofibers of an approximate diameter of 4 nm observed in Transmission Electron Microscopy (TEM) (Kiss et al., 1987), arranged in a concentric pattern

in the paramylon granules. The estimated native crystallinity index is close to 88% (Marchessault & Deslandes, 1979). In comparison, curdlan, which shares the same linear β-1,3 structure is only 30% crystalline and is partially soluble in water due to the presence of a fraction of mono helices in its native state, allowing the formation of gels by a subsequent rearrangement of the chains from solution (Y. Chen & Wang, 2020).

The stability of paramylon's native crystalline structure impedes thermoplastic processing without thermal degradation: the only reported attempt of hot-press compression moulding of hydrated paramylon granules lead to a so-called "resinification" at temperatures above 200°C with partial thermal degradation and uncontrolled crosslinking reactions (Kawahara et al., 2020). In the 220 to 240°C moulding temperature range, X-ray diffraction (XRD) analysis showed that the native paramylon crystal peaks become broadened after hot-pressing, and that new peaks appear, suggesting a new unknown crystalline structure (Kawahara et al., 2020). To our knowledge, thermoplastic behavior without thermal degradation or crosslinking was only reported for paramylon monoesters and mixed-esters derivatives (Shibakami et al., 2014) (Shibakami & Sohma, 2017) (Gan et al., 2017) (Shibakami & Sohma, 2018).

The few known solvents able to disrupt the triple helices and to fully dissolve paramylon chains as random coils without depolymerisation have either extreme basic pH, such as concentrated aqueous NaOH (Shibakami et al., 2013), or strong hydrogen bonding ability, such as DMSO (Futatsuyama et al., 1999)(Kawahara & Koganemaru, 2006). and DMAc/LiCl (Shibakami et al., 2014). Recently ionic liquids (IL) were highlighted as a new family of solvents: A mixture of 1-butyl-3-methylimidazolium chloride ([Bmim][Cl]) with a DMAc ([Bmim][Cl]:DMAc volume ratio of 5:2) was first shown to solubilize paramylon (Yasuda et al., 2018).

In the present work, we show the feasibility of using a mixture of a biocompatible IL with water as a plasticizer for the formulation of thermoplastic paramylon without chemical modification of the biopolymer. This proof of concept for paramylon non derivatizing melt-processing is inspired by previous studies on thermoplastic starch (TPS). Indeed TPS can be formulated from native starch granules mixtures using ILs as plasticizers in presence of water. Such ILs are based on different cations such as imidazoliums (Sankri et al., 2010; Xie et al., 2014) and choliniums (Colomines et al., 2016; Decaen et al., 2017). Moreover, it was shown that water:[1-ethyl-3-methylimidazolium][acetate] mixtures allow the melt processing of thermoplastic starch below 100°C, with processing as low as 55°C for a 54:60 water:IL ratio (Zhang et al., 2017). This result may be ascribed to a synergy between the two plasticizing components that was also observed during starch solubilization experiments in water mixtures with the same imidazolium IL (Mateyawa et al., 2013), as well as with choline based ILs (Sciarini et al., 2015).

In the case of the biocompatible IL selected for the present work on paramylon plasticization, cholinium glycinate ([Cho][Gly]) (De Santis et al., 2015), it was recently shown that 40:60 water:IL mixtures are able to solubilize starch at temperatures lower than 70°C (J. Chen et al., 2021). This was ascribed to the presence of water-separated ion pairs allowing $[Cho]^+$ and $[Gly]^-$ to efficiently interact with starch repeating units (J. Chen et al., 2021). Therefore, our assumption was that it may also efficiently interact with paramylon, which as the same glucosidic repeating unit.

2) Materials and methods

2.1) Materials and formulations

Paramylon was purchased from Sigma Aldrich in the form of a crystalline white powder with a water content of 3% (measured by Thermogravimetric Analysis (TGA)). Its average molecular weight, 130 kDa, was evaluated by viscosimetry in solution in Dimethylsulfoxyde (DMSO) (Futatsuyama et al., 1999).

Cholinium glycinate ([Cho][Gly]) IL was synthesized by an acid/base reaction between Choline hydroxide and glycine (both purchased from Sigma Aldrich), as described in literature (De Santis et al., 2015). Briefly, the reaction was conducted in water at 25°C during 24h under stirring and nitrogen atmosphere. Excess water was then removed under vacuum at 50°C before precipitation of [Cho][Gly] by adding absolute ethanol. After filtration to remove any unreacted amino acid, the final product (purity 95%) was dried under vacuum for 48h at 50°C. Chemical structure was confirmed by Nuclear Magnetic Resonance (^{1}H NMR (500 MHz, D_2O) δ/ppm: 3.04 (s, 9H, $(CH_3)_3N$), 3.07 (s, 2H, CH_2NH_2), 3.39 (m, 2H, CH_2OH), 3.92 (m, 2H, CH_2CH_2N).^{13}C NMR (500 MHz, D_2O) δ (ppm): 44.7, 53.8, 55.5, 67.4, 180.7.).

A water:IL mixture (40:60 mass ratio) was first prepared by mixing ([Cho][Gly]) with deionized water under stirring during 10 min. at 25°C. This liquid mixture was used for paramylon solubilization tests and for the preparation of two paramylon:water:IL wet powder batches (with two levels of plasticizer) for extrusion and hot press processing. The liquid mixture was added dropwise to pristine paramylon powder at 25°C and mixed in a mortar in order to obtain batch #1 (containing 100 part of paramylon, 40 part of water and 60 part of IL) and a less plasticized, batch #2 (containing 100 part of paramylon, 30 part of water and 45 part of IL.) These wet powder batches was stored at 5°C before characterizations and processing.

2.2) Solubility of paramylon in water:IL mixture

Tests were conducted by heating at 80°C dilute (2%) and concentrated (10% and 20%) suspensions: i). The dilute solution was prepared in a flask, using a magnetic stirrer: Paramylon powder was dispersed in the water:IL mixture in order to obtain a 2% w/w suspension, which was heated at 80°C during 60 min. and then cooled at 20°C. ii) For the concentrated solutions, paramylon powder was dispersed in the water:IL mixture in order to obtain 10% w/w and 20% w/w suspensions, which were introduced in a rotational rheometer (HAAKE MARS III) equipped with a Peltier temperature control system and a plate-plate geometry (∅ 20 mm). A dynamic deformation of 1% was applied with a frequency of 1Hz, with the following temperature program: 60 s isotherm at 20°C, heating ramp from 20°C to 80°C at 1 K.min^{-1}, 600 s isotherm at 80°C, cooling ramp from 80°C to 20°C at 1 K.min^{-1}, 600 s isotherm at 20°C.

2.3) Thermo-mechanical processability of paramylon:IL:water wet powders:

The thermoplasticity of batch #1 and batch #2 was evaluated by extrusion and hot press experiments. Extrusion was simulated using a laboratory scale twin screw microcompounder at 95°C (Minilab, HAAKE, Thermo Haake). This conical twin screw system equipped with a backflow channel allows the mixing of approximately 8 g of wet powder during a controlled residence time, which was fixed to 200 s after filling the recirculating cavity, before extrusion. Screw speed was 100 rpm. The torque signal was recorded and used to calculate the Specific Mechanical Energy (SME) (J g^{-1}):

$$SME = \int_0^t \frac{2\pi.n.C}{60.M} dt \qquad (1)$$

Where : n is screw speed fixed to 100 rpm, C is the torque signal (N.cm) at mixing time t, and M is the loaded mass.

Concurrently, the pressure drop signal in the backflow channel, ΔP, was also recorded, and used to evaluate the apparent viscosity of the material. Since the backflow channel's thickness (h= 1.5 mm) is small in comparison to its width (w = 10 mm), the shear stress τ_w at the wall of the channel and the apparent shear rate $\dot{\gamma}_{app}$ can be evaluated as follows (Son, 2007):

$$\tau_w = \frac{h \times \Delta P}{2 \times \Delta L} \times \left(\frac{1}{\frac{h}{w}+1} \right) \approx \frac{h \times \Delta P}{2 \times \Delta L} \qquad (2)$$

$$\dot{\gamma}_{app} = \frac{6 \times Q}{w \times h^2} \qquad (3)$$

Where ΔL = 64 mm is the distance between the pressure sensors and the flow rate in the recirculation channel, Q [$m^3.s^{-1}$], is assumed proportional to the screw speed n (rpm): Q = C.n, with C = 6.10^{-10} m^3 s^{-1} rpm^{-1} is a calibration constant that was obtained in a previous study (Decaen et al., 2020). So finally, the apparent viscosity is given by:

$$\eta = \frac{\tau_w}{\gamma_{app}} \qquad (4)$$

Concurrently, hot press compression molding was conducted at 95°C (20 MPa, 10 min.) using a steel spacing circular frame of thickness 0.5 mm between two Teflon sheets. After processing, all samples were stored at 25 °C under a controlled relative humidity of 59% (using a reference saturated sodium bromide salt solution) before and between characterizations.

2.4) Characterizations of pristine paramylon, wet powders and thermoplastic paramylon.

All samples were characterized using Wide Angle X-ray Scattering (WAXS) using a Bruker D8 Discover diffractometer with a recording time of 10 minutes. The IμS microfocus source equipped (radiation Cu Kα1 = 1.5405 Å)) with MONTEL optics provides a small high intensity x-ray beam at 50 kV and 1 mA, collimated to produce a 500 μm beam diameter. X-ray diffraction data were collected using a Bruker Vantec500 two-dimensional detector. Samples are placed between two sheets of tape.

Additional characterizations in Small Angle X-Ray Scattering (SAXS) were performed on extruded and hot pressed samples using the same setup but with a sample-detector distance of 300 mm. The orientation of the diagram was evaluated for these SAXS measurements.

The infrared absorption spectra of paramylon, IL, wet powder and hot pressed films were obtained with a resolution of 1 cm−1 in the 700–4000cm−1 wave number range, using a Fourier Transform Infrared (FTIR) Spectrometer (Tensor 27, BRUKER) equipped with an Attenuated Total Reflection system (ATR, PIKE). The OPUS® software was used for the analysis of the IR absorption spectra, especially for the identification of peak maxima.

Microscopic observations were performed on the hot pressed films: Scanning Electron Microscopy (SEM) was used to observe the surface and cross-sectional morphology of the films using a JEOL 7000F FE-SEM (JEOL, Peabody,USA) at an accelerating voltage of 10 kV. Fracture surfaces were obtained by cooling the films in liquid nitrogen followed by brittle break.

Transmission Electron Microscopy (TEM) experiments were carried out using the Nant'Themis, a (S)TEM Themis Z G3 Cs-probe corrected microscope (Thermo Fisher Scientific) operated at 80 kV and at low temperature, 96K. Samples for TEM analysis were prepared using a cryo-ultramicrotome (Leica UC7/FC7) equipped with diamond knife (Diatome), at 193K.

Freshly hot pressed and 1 month old films were analyzed by Differential Scanning Calorimetry (DSC Q200, TA instruments). The DSC instrument was calibrated with an indium standard. Analyses were made with 12–13mg samples, using hermetically-sealed aluminum pans. An empty pan was used as a reference. Samples were cooled down to −80°C (the lowest temperature possible for the apparatus) at -3K.min^{-1} and heated at 3K.min^{-1} up to 95°C, then cooled again down to -80°C at -3K.min^{-1}, and heated at 3 K.min-1 up to 130°C.

The thermomechanical behavior of films was evaluated by tensile tests at 20°C and by dynamic mechanical thermal analysis using a DMA apparatus (Q800 from TA Instruments) in tensile small deformation mode (0,1% at 1 Hz). Samples cut from the films of typical dimensions 20 mm × 8 mm × 0.4 mm were placed in the DMA apparatus at 20°C and cooled at -70°C, before

recording the evolution of the storage modulus E'(MPa), the loss modulus E''(MPa) and the tangent of loss angle tan δ =E"/E'during a temperature ramp from -70°C to 130°C at 3K.min^{-1}. The initial water content in the film was evaluated by placing samples in an oven at 130°C during 3 hours, and measuring the mass loss.

Due to limited availability of paramylon, large deformation tensile tests was only performed on films obtained by hot pressing of batch #2: ASTM D412 type dogbone samples cut from the films were tested using an INSTRON 1122 universal press at 10 mm/min. The strain was defined as the ratio of the displacement of cross-head x to the initial length of the sample l_0 :

$$\varepsilon = \frac{x}{l_0} \qquad (5)$$

The stress was defined as the ratio of the force F to the initial section of the sample $\mathbf{S_0}$:

$$\sigma = \frac{F}{S_0} \qquad (6)$$

The stress–strain curves were analyzed in order to obtain the elongation at break (%), the stress at break (MPa) and Young's Modulus (MPa).

3) Results and discussion

3.1) Characterization of the wet powder batches

Figure 1 shows the WAXS diffractograms obtained for the pristine paramylon powder, and for the wet powders obtained after mixing with the water:IL system. It is striking that all the diffraction peaks of paramylon completely vanish in the wet powder. The peaks for pristine paramylon have been indexed in **Table 1** considering the native hexagonal crystalline structure reported in literature for paramylon (Kobayashi et al., 2010). An almost perfect match between observed and predicted interplanar spacings can be observed, for unit cell dimensions a = 14.76 Å and c= 5.84 Å, which are consistent with a partially hydrated structure (Kobayashi et al., 2010).

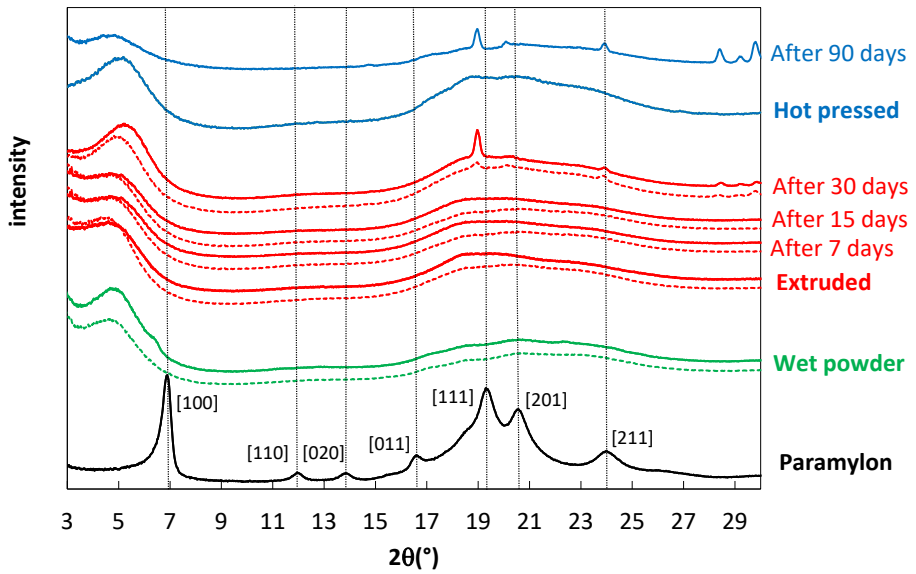

Figure 1: WAXS diffractograms for pristine paramylon and formulations with the water:IL system before and after thermomechanical processing for batch #1 (dotted lines) and batch #2 (continuous lines). Vertical black dotted lines indicate the position of the peaks for paramylon.

Table 1: Diffraction peaks indexation for pristine paramylon and wet powder batches. Expected spacing values are calculated for hexagonal unit cell dimensions a = 14.76 Å and c= 5.84 Å (*), and taken from literature (**).

2θ (°)	**hkl**	**spacings (Å)**	
		observed	predicted
Paramylon			
6.91	100	12.78	12.78 *
12.00	110	7.37	7.38 *
14.00	020	6.32	6.39 *
16.68	011	5.31	5.31 *
19.34	111	4.59	4.58 *
20.61	201	4.31	4.31*
23.96	211	3.71	3.72 *
Wet powders (batch #1 and batch #2)			
4.75	Triple helix pitch	18.59	18.59 **

For the wet powders of batch #1 and #2, a broad peak centered on 4.75° (18.59 Å.) appears, which corresponds to the pitch of a paramylon triple helix, usually observed in hydrated crystals (Kobayashi et al., 2010) (**Table 1**). To our knowledge, such a peak has never been reported before for paramylon. However, it has been reported for schizophyllan, another linear β,1-3 glucan, which due to the presence of one β,1-6 glucosyl side-chain on every three glucosidic unit of its backbone, takes a similar triple helix conformation but cannot form hexagonal crystals (Kono et al., 2020).

In the wet powders, the fact that paramylon's native hexagonal packing of triple helices vanishes due to the presence of the IL, suggests strong interactions between the glycosidic units and the ions. The FTIR results on **Figure 2** support this assumption. The main absorption peaks indexed **Table 2** correspond to those previously reported for pristine paramylon (Noble et al., 2020) or curdlan that shares the same macromolecular structure (Mangolim et al., 2017) and for cholinium glycinate (J. Chen et al., 2021; Tao et al., 2013). In the 800-1700 cm^{-1} range (**Figure 2a**), several peaks observed for the wet powder spectrum can be ascribed to paramylon or to the IL present: Considering the peaks of paramylon: only the one at 1153 cm^{-1} remains unchanged in the wet powder, while all the other peaks are shifted either toward higher or lower wavenumbers (**Table 2**). For the peaks corresponding to non-polar groups, this may be ascribed to a higher mobility to the absence of crystallinity, while for the peaks corresponding to polar groups involving oxygen, this indicates a change of their hydrogen bonding environment. By assuming a simple harmonic oscillator model, these shifts respectively indicate an increase, or a decrease, of the hydrogen bonding to which the functional groups of paramylon are submitted in presence of the IL, compared to the native crystals. In the case of the peak at 1041 cm^{-1} attributed to CO, it is apparently separated into two peaks in the wet powder, on shifted at 1034 cm^{-1} and the other not significantly shifted at 1043 cm^{-1}, which may be ascribed to the presence of two populations, forming, and not forming, hydrogen bonds with the IL.

Concurrently, similar shifts can be observed for the peaks of cholinium glycinate, in particular for the two COO^- peaks at 1399 cm^{-1} (upshifted at 1402 cm^{-1}) and 1576 cm^{-1} (downshifted at 1566 cm^{-1}). This behavior similar to what has been reported for water:IL mixtures due to hydrogen bonding with water (J. Chen et al., 2021). In our case, hydrogen bonds with paramylon are also likely to be present.

In the 2800-3600 cm^{-1} range (**Figure 2b**), a shift of the maximum of the large OH peak in the 3000-3600 cm^{-1} toward lower wave numbers is observed. However, it is not possible to analyze in detail the shifts of the peaks of paramylon and IL, which are strongly overlapped.

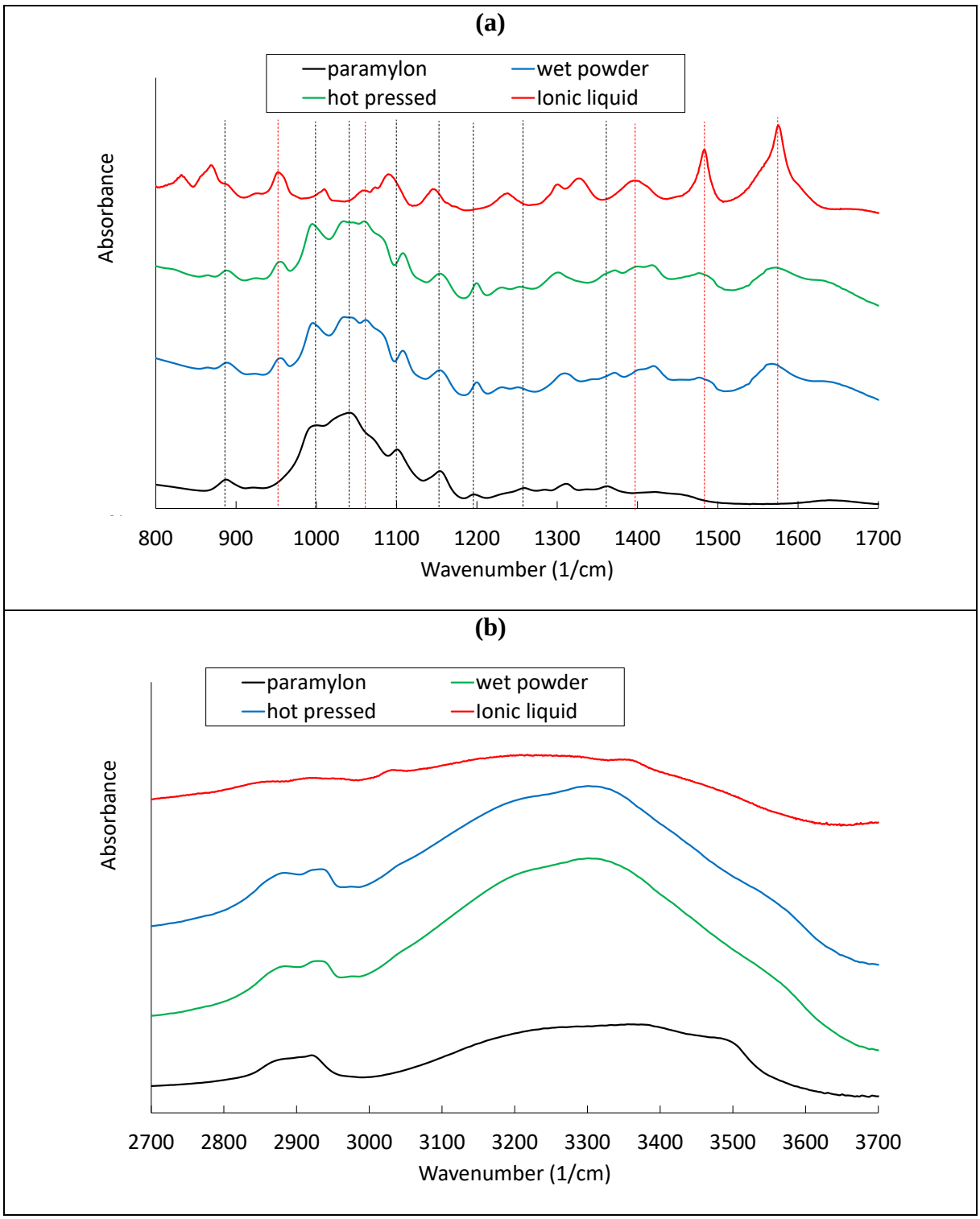

Figure 2: Infrared absorption spectra of paramylon, IL, and batch #2 (before and after hot pressing.) in the 800-1700 cm^{-1} (**a**) and 2700-3700 cm^{-1} (**b**)

Table 2: FTIR absorption peaks in the 800-1600 cm^{-1} range (arrows indicate the absence (→), or presence of shifts toward lower (↓) or higher (↑) wavenumbers.

Position of peak maximum (cm^{-1})			**Group**
Paramylon	**Wet powder**	**Hot pressed**	
887	889 ↑	889 ↑	C_1H of β linkage
1001	996 ↓	994 ↓	C-O stretching or bending
1041	1034 ↓ +1043→	1034 ↓ + 1045 →	C_1-O-C_5 stretching or bending
1100	1107 ↑	1107 ↑	O-H stretching or bending
1153	1153 →	1153 →	C_1-O-C_3 stretching or bending
1196	1200 ↑	1200 ↑	OH bending
1260	1250 ↓	1250 ↓	C-H bending or CH_2 wagging
1362	1372 ↑	1372 ↑	C-H bending
IL	**Wet powder**	**Hot pressed**	**group**
952	957 ↑	957 ↑	N-$(CH_3)_3$ stretching
1060	1060 →	1059 →	CH_2-OH asymmetrical deformation
1399	1402 ↑	1402 ↑	COO^- symmetric stretching
1484	1476 ↓	1476 ↓	CH_3 asymmetrical deformation
1576	1566 ↓	1572 ↓	COO^- asymmetric stretching

3.2) Solubilization tests

In dilute conditions (2% w./w. of paramylon), a homogenous solution was obtained at 80°C as can be seen on the photograph included in the graphical abstract, indicating its complete solubility in the water: IL mixture. After cooling at 20°C, no precipitation was observed, but a gel was formed after storage overnight, as can be seen on the graphical abstract. Due to its high ion content (≈ 60% w./w.), it is actually an ionogel that is obtained, a type of material that was previously reported for cellulose solutions in ILs (Hopson et al., 2021). The gelation phenomenon is reversible: Heating the gel at 80°C leads to a homogeneous solution, which forms again a gel upon cooling at 20°C. This suggests a solubilisation of the paramylon chains as random coils at 80°C, and their subsequent rearrangement as triple helix conformers forming a network of nanofibers after cooling. Indeed, paramylon is known to be able to reform triple helices and nanofibers by self-assembly from solution (Shibakami et al., 2013). The formation of gels due to this self-assembly property has been reported for water-soluble cationic paramylons with a low degree of substitution (Shibakami et al., 2018).

For the tests at 10% and 20% w./w. of paramylon, **Figure 3** shows the evolution of the storage (G') and loss (G") moduli measured with the rheometer: Initially, at 20°C the rheological behaviour is typical of concentrated suspensions of hard spheres, with G' > G''. The moduli are rather close for the 10% suspension (G'≈ 0.75 kPa; G'' ≈ 0.56 kPa); while an essentially elastic behaviour is observed for the 20% suspension (G'≈ 23 kPa; G'' ≈ 7 kPa). During the heating ramp, the storage modulus G' of the two suspensions first increased with temperature, but then decreases dramatically above 60°C. Such a behaviour is similar to that observed for a 10% starch suspension in the same water:IL mixture in which starch granules first swell, before being disaggregated, leading to homogeneous starch solutions (J. Chen et al., 2021). Therefore, we can assume a similar scenario in which paramylon particles are first swollen by the water:IL mixture, before being disaggregated and at least partially solubilized, between 60°C and 80°C. However, the fact that G' remains higher than G'' at 80°C suggests a transition from a suspension to a gel, due to the high concentration of paramylon. The continuous increase of the moduli observed during the subsequent cooling ramp, up to G' ≈ 13.6 KPa, and G" ≈ 2.4 KPa at 20°C for the 10% solution (and up to G' ≈ 46.2 KPa, and G" ≈ 9.5 KPa at 20°C for the 20%

solution) may be ascribed to the rearrangement of the paramylon chains as a dense network of triple helix based nanofibers, similarly to what is observed for curdlan gels (Y. Chen & Wang, 2020).

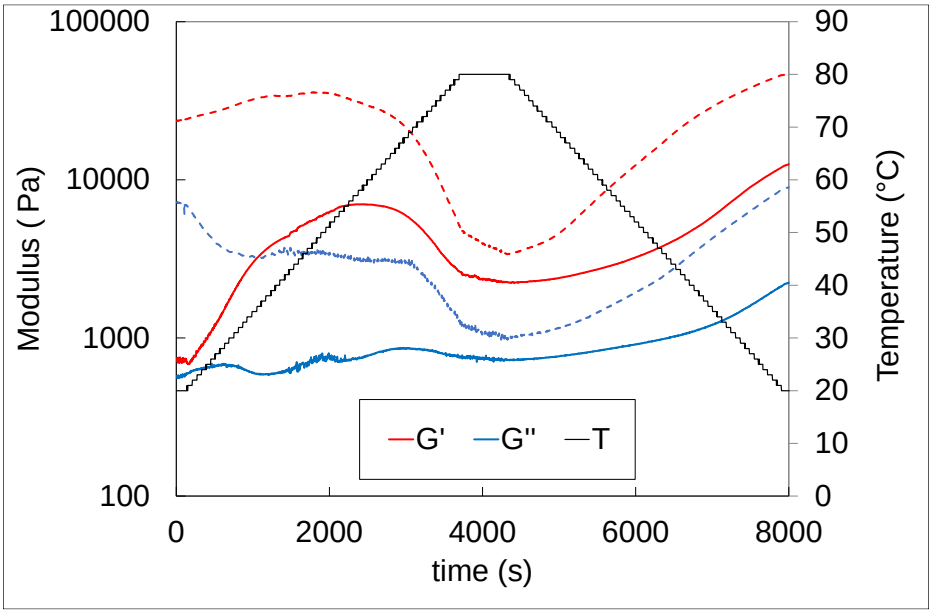

Figure 3: Thermo-rheology of concentrated solutions of paramylon in water:IL mixture, starting from a 10% w./w. suspension (continuous lines) and a 20% w./w. suspension (dotted lines).

3.3) Extrusion and hot pressing at 95°C

The two wet powder batches were successfully extruded and hot pressed at 95°C. **Figure 4** shows the signals monitored during processing with the twin-screw microcompounder: After filling the recirculating cavity, the torque and pressure drop in recirculating channel roughly stabilized during the recirculation step. The estimated Specific Mechanical Energies (SME) and apparent viscosities were respectively 540 kJ/kg and 2.5 kPa.s (at $16s^{-1}$) for batch #1; and 1242 kJ/kg and 5.4 kPa.s (at $16s^{-1}$) for batch #2. The higher values for this latter may be ascribed to the higher paramylon content in the wet powder (57% of paramylon for batch #2 compared to 50% w/w for batch #1). However, due to the very high plasticizer content in both cases (respectively 50% and 43% of IL:water mixture, that is to say 37.5% and 31%% IL based on paramylon dry weight), the viscosities are lower than what was previously reported for thermoplastic starches plasticized with glycerol or ILs at 130°C (between 5 and 12 kPa.s for 74% of starch w/w) (Decaen et al., 2020).

The extruded rods were translucent (**Figure 5a)**, while the hot pressed films were transparent **(Figure 5b**), both with a yellowish color similar to that of the IL. After extrusion or hot pressing, the WAXS diffractograms remained unchanged compared to the wet powders (**Figure 1**) as well as the position of the main FTIR peaks (**Table 2**). SEM observations of the cross section of hot pressed films after 7 days show a fracture surface typical of an amorphous matrix (**Figure 5c**) However, the SEM image suggests the presence of an outer layer different from the core. This may be the result of a change of water content at the surface of the films during processing.

Concurrently TEM observations through slices parallel to the surface of the films tend to show the presence of lower density domains of size ranging approximately from 50 to 200 nm, within a higher density fibrous like network. The thickness of these darker fibrous domains apparently ranges between 10 to 20 nm, which corresponds to the diameter of paramylon nanofibers formed by self-assembly of triple helices (Shibakami et al., 2013). Concurrently, the lower density domains may be ascribed to amorphous matrix regions between the nanofibers.

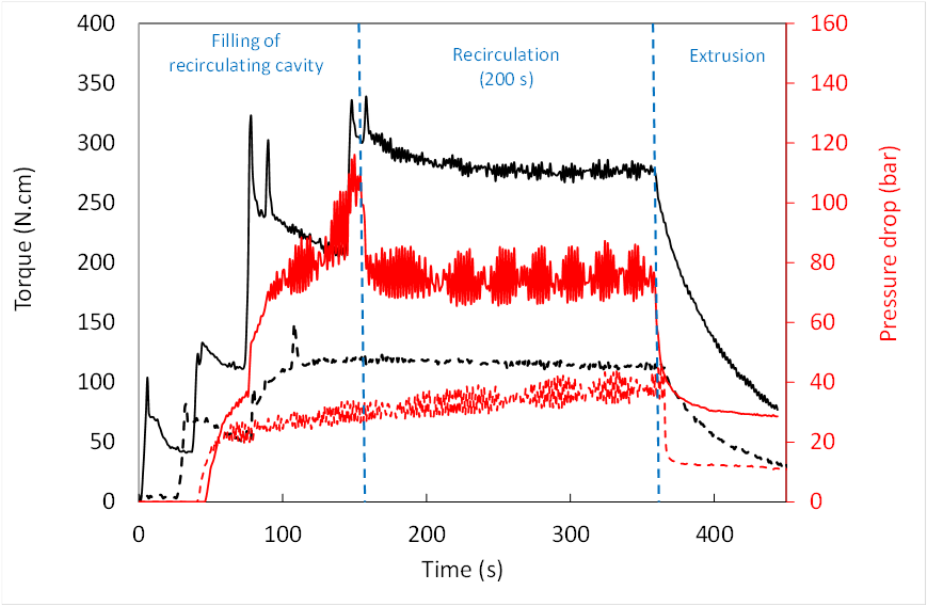

Figure 4: Extrusion at 95°C: Torque and Pressure drop signals recorded with the twin screw microcompounder for batch 1 (dotted lines) and batch 2 (continuous line).

The SAXS diffractograms (**Figure 6**) actually show that depending on plasticizer content and processing conditions (extrusion or hot press) the structure of samples varies: For all samples, a main peak is observed at a distance d ranging from 17.8 to 19.1 Å, corresponding to the triple helix pitch (as observed in WAXS), a second peak, much broader and centered around $d \approx 42$-45 Å is also observed, rather strong for the hot pressed samples, and much weaker for the extruded samples (**Figure 6a**).

This second peak may correspond to a higher order peak associated to the triple helix pitch (along the nanofibers axis), or more probably to the radial packing of the triple helices in the nanofibers: Indeed, it was reported that in native paramylon granules, the triple helices are primarily packed as nanofibers having a diameter of 40 Å (Kiss et al., 1987), that form larger bundles. Such 4 nm diameter subunits were actually also observed inside 20 nm paramylon nanofibers formed by self-assembly (Shibakami et al., 2013). Therefore, it may be assumed that the 10-20 nm thick nanofibers observed in TEM in hot pressed samples may be composed of such 4 nm thick smaller nanofibers, leading to the broad peak observed in SAXS. It may be further assumed that depending on the processing conditions, this native nanofiber structure can be partially preserved in particular for a low viscosity formulation and low shear conditions, which is the case of the hot pressed samples. As an opposition for a high viscosity formulation, processed with high shear, which is the case of the extruded sample (particularly batch #2), the native packing of 4nm thick nanofibers as thicker nanofibers is likely to vanish completely, explaining the much lower intensity of the peak around 42-45 Å (**figure 6a**).

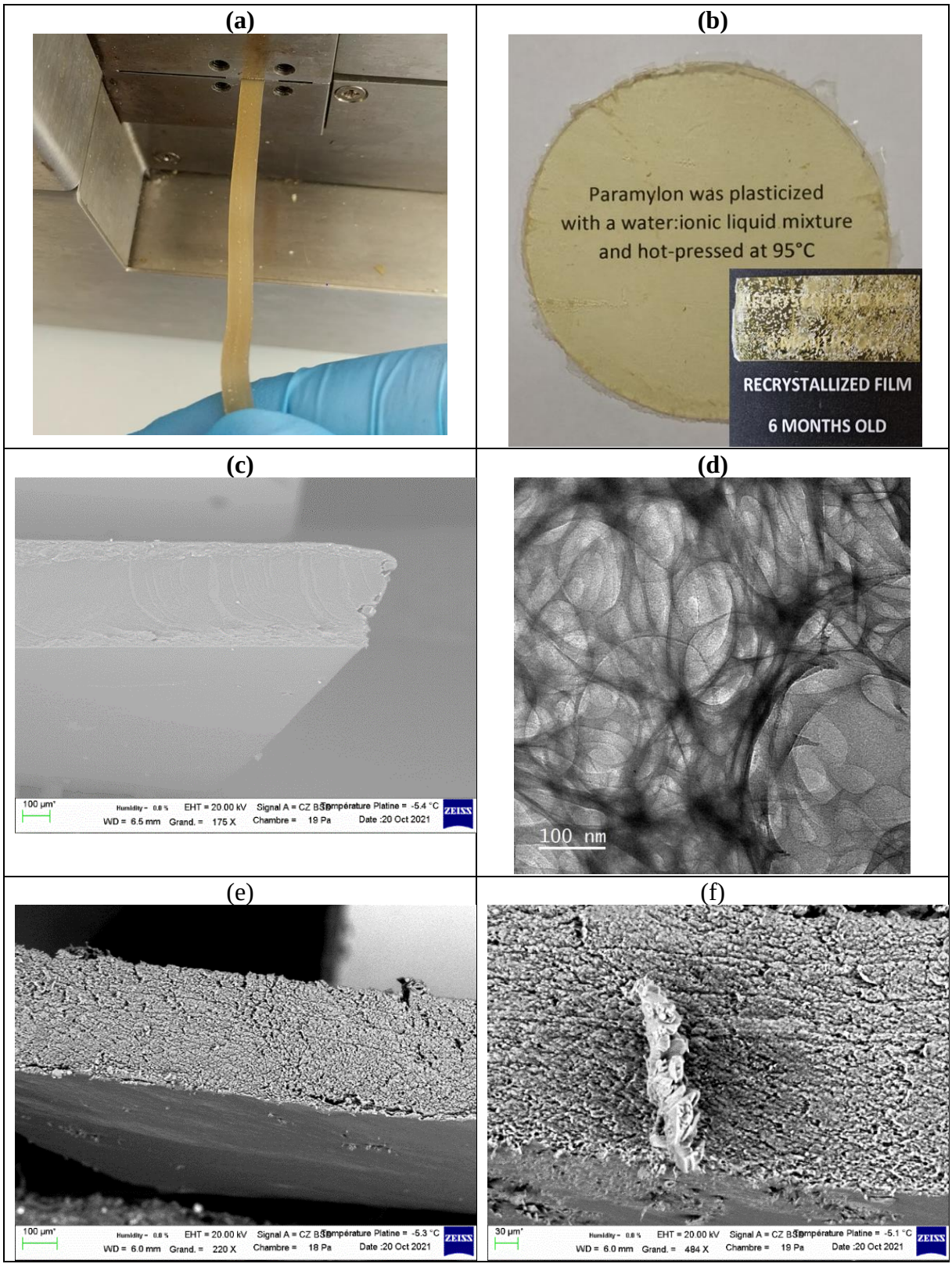

Figure 5: Photos of extruded (a) and hot pressed samples (b), SEM and TEM observations of hot pressed samples, seven days after processing (c, d); and SEM observations 6 months after processing (e, f)

The scattered intensity variations depending on azimuthal angle α (**Figure 6b**), show that plasticizer content and processing conditions affect the orientation of nanofibers. The strongest orientation is observed for the hot pressed samples, with maximum intensities at α = +90°/-90° for batches #1 and α= +130°/-50° for batch#2. Assuming that these maxima correspond to the strongest intensity peak around 42-45 Å (**figure 6a**), ascribed to the packing of 4nm thick nanofibers perpendicularly to their axis, this suggest a preferential orientation of the nanofibers axis in the plane of the films, along the 0° direction for batch#1 and along the 40° direction for batch #2.

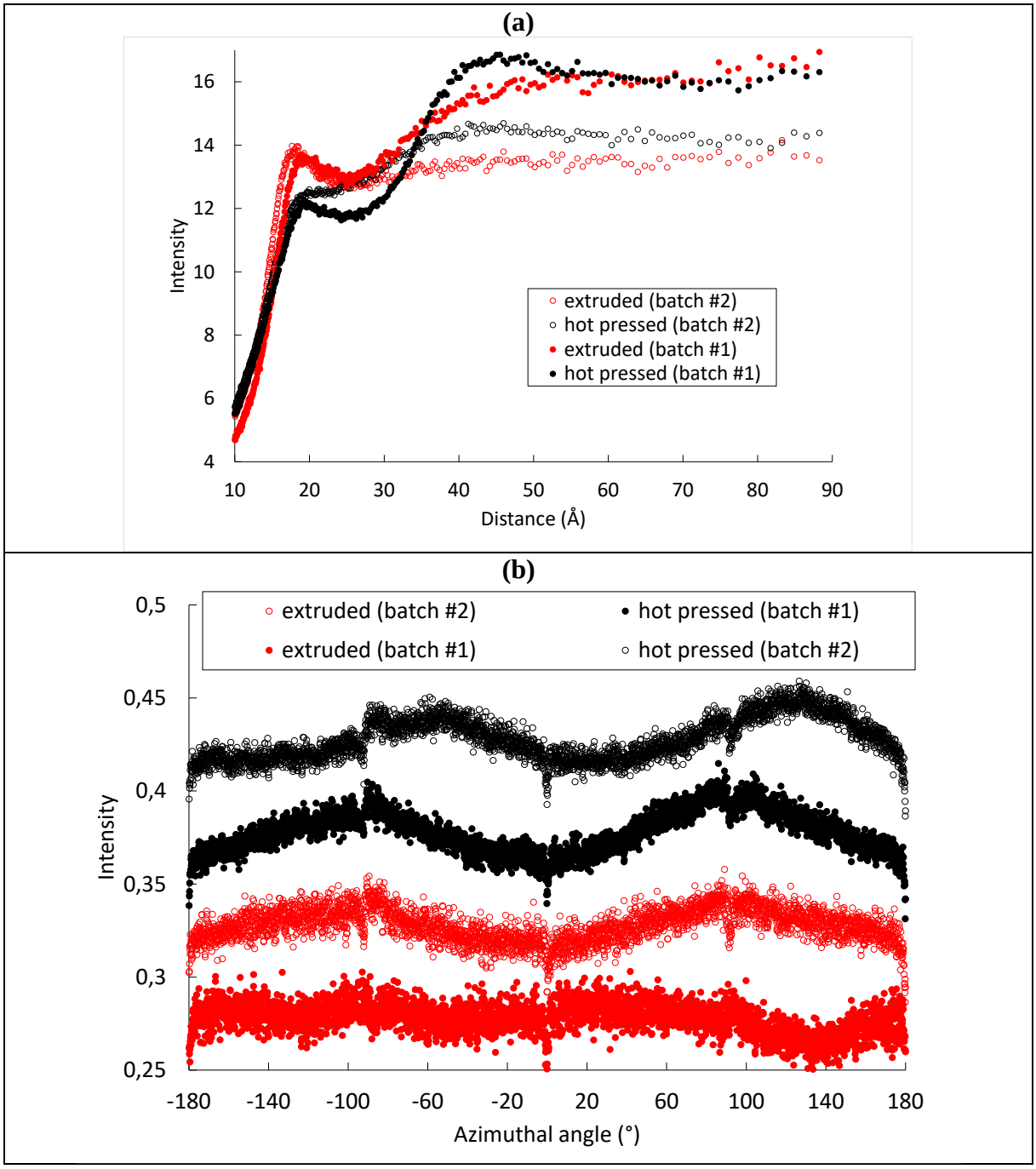

Figure 6: SAXS on extruded and hot pressed samples: Scattering intensity (a) and orientation (b). Extruded rods are oriented vertically (flow direction along 90° azimuthal angle)

Taking into account that the circular metallic frame molding used as spacer for hot pressing results in films that have the shape of a disc, and that the samples were cut on the hedges of these film discs, these observations are compatible with a radial orientation of the nanofibers. During hot press processing, we assumed that the 10 minutes compression molding time is likely to allow the flow and relaxation of the amorphous matrix, resulting in the orientation of nanofibers in the radial flow direction. This raw assumption is based on our previous experience on IL plasticized starch films, for which a 5 minutes compression molding time was enough for flow and relaxation (Decaen et al., 2017). However, in future works, it would be interesting to investigate the influence of the compression molding time on paramylon nanofibers' orientation.

For the extruded sample of batch#2, clear maxima at α= +90°/-90° are observed on **Figure 6b**. However, for this sample, the strongest peak on **Figure 6a** is the peak around 18 Å ascribed to the triple helix pitch (the second peak at 42-45 Å being very weak). Thus it suggests an orientation of the triple helices' axis along the vertical extrusion flow direction (aligned with the direction α= +90°/-90°).

For the extruded sample of batch #1, no clear pair maxima appear on **Figure 6b** (though an absolute maximum seems present at α= -90° and a local maximum at α= +90°). This may be due either to a much lower flow induced orientation of the triple helices/nanofibers as a result of lower viscosity and lower shear during extrusion compared to batch#2; or to the fact that the two peaks around 18 Å and 42-45 Å have similar intensities (**Figure 6a**), resulting in an apparent lack of orientation when integrating the signal.

3.4) Thermal, thermomechanical and tensile properties of hot pressed films

Mechanical characterizations were performed on films 7 days after hot pressing and storage at 59% RH. We assumed that this storage time was long enough for the water content in the plasticized paramylon films to reach equilibrium. According to our previous experience on starch films plasticized by ionic liquids and water, such an equilibrium is typically reached in less than 4 days (Sankri et al., 2010).

The water content in the films before DMA was evaluated by mass loss at 130°C during 3 hours. The observed mass loss was 23% for batch#1 and 21% for batch#2. These values are actually close to the initial water contents in wet powder batches (respectively 25% for batch#1 and 21% for batch#2). However, the samples, initially transparent, became opaque with a dark brown color, suggesting a simultaneous partial thermal degradation of the material. TGA analysis (**supplementary Figure A**) actually confirmed that the hot pressed films were significantly less thermally stable than pristine paramylon. This may be ascribed to the low thermal stability of cholinium based ILs (Colomines et al., 2016).

DSC and DMA results are presented on **Figure 7.** No significant difference is observed between the first and second heating ramp in DSC. The thermal and thermo mechanical behavior of the films appears quite complex, but may be rationalized assuming the presence of two phases, in agreement with the structural characterization results: An amorphous matrix, and a reinforcing phase consisting of nanofibers and/or individual triple helices.

At -70°C, a very high modulus of approximately 6 GPa is observed for the two batches, followed by a large relaxation between -70°C and 20°C, centered on $T_\alpha \approx$ -33°C for batch #1 and $T_\alpha \approx$ -39°C for batch #2. Given the strength of this relaxation, we assume that it corresponds to the amorphous matrix. Following this assumption, the decrease of heat flux (i.e. increase of heat capacity) observed in DSC thermograms between -80°C and -30°C, may be ascribed to a first glass transition, starting below the temperature range accessible with the DSC apparatus at our disposition. (In the case of batch #2, displaying a lower T_α, the glass transition probably

starts well below -80°C, explaining the relative low decrease of heat flux compared to batch #1 on the thermograms).

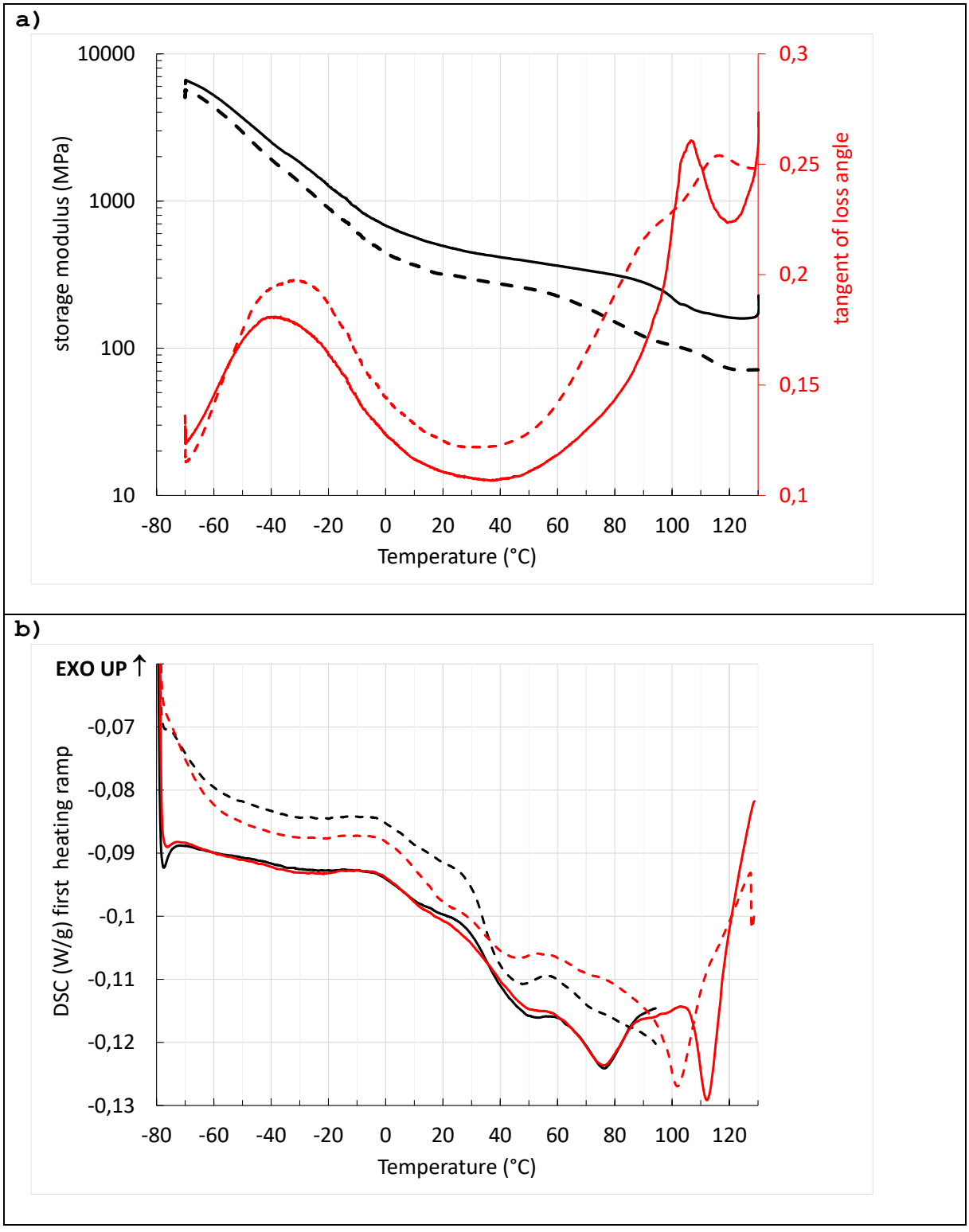

Figure 7: Thermomechanical and thermal properties hot pressed films of batch #1 (dotted lines) and batch #2 (continuous lines), obtained in DMA (a) and DSC (b, black and red lines correspond to the first and second heating ramp, respectively)

A slowly decreasing plateau is observed above 20°C, with $E'_{30°C} \approx 293$ MPa for batch #1 and $E'_{30°C} \approx 445$ MPa for batch #2. These values are consistent with the assumption of the presence of triple helices and/or nanofibers, reinforcing the rubbery amorphous matrix. The modulus of the batch #2 film at 30°C is actually very close to the value of 500 MPa reported for paramylon hot pressed at 220°C without plasticizer (and partially degraded/ crosslinked) (Kawahara et al., 2020).

We assume that the other thermal events and mechanical relaxations below 100°C may be ascribed to the reinforcing nanofibers/triple helices phase: Indeed, between 0°C and 50°C, the two batches present a similar wide heat flux drop (i.e. increase of heat capacity) that may be ascribed to a glass transition phenomenon with an overall "mid point" $T_g \approx 20$°C for batch #1 and $T_g \approx 30$°C for batch #2. However, this increase of heat capacity seems to take place in two steps, with a first drop of heat flux starting around 0°C, and a second drop starting around 30°C. This complex behavior may be due to the presence of not only one broad glass transition, but of two subsequent glass transitions phenomena.

The secondary mechanical relaxations observed on DMA curves (with a drop of the modulus above 60°C for batch #1, leading to a second plateau modulus $E'_{100°C} \approx 100$ MPa; and above 80°C for batch #2, leading to a second plateau modulus $E'_{120°C} \approx 160$ MPa) may be related to these glass transitions. However, melting phenomena may also be involved, as endothermic peaks are observed around 45°C for batch #1 and around 75°C for batch #2. Recalling the solubilization tests results, this second relaxation thus may be associated to a partial melting of the triple helices.

Additional endothermal peaks are observed for the second heating ramp, around 102°C and 112°C for batch #1 and batch #2, respectively. For batch #1, a third mechanical relaxation leading to a third plateau ($E'_{120°C} \approx 70$ MPa) is observed in this high temperature range, which may be correlated to the endothermic peak. However, above 100°C water loss may take place, as well as partial thermal degradation. Indeed, after completing the DMA experiments, the films had taken a similar opaque, brown colored aspect as those dried at 130°C for water content estimation.

Recalling the SAXS results showing structural differences between the films, these differences in thermal and thermomechanical behaviors may be ascribed to process induced structural changes of the reinforcing phase, that would lead to more stable nanofibers for batch #2. This assumption may be a starting point for future studies on the influence of process parameters on thermoplastic paramylon films' structure and properties.

For batch #2, the large deformation tensile properties at 25°C were also characterized, showing a ductile behavior (**supplementary figure B**). The tensile mechanical properties are given in **Table 3** and compared to available literature data for paramylon and curdlan films obtained by casting from solution or by hot press (with partially degradation/crosslinking). The thermoplastic IL:water plasticized paramylon film shows the highest elongation at break. However, due to the absence of plasticizer in most of these previous works, the Young's modulus and stress at break values are much higher than for our samples, in which 43% of water:IL mixture is used as a plasticizer. The closest values are reported for a 30% glycerol plasticized curdlan film. In future studies, it would be interesting to investigate lower IL:water contents in order to increase the modulus, or other potential ionic plasticizers already investigated for starch such as other ILs (Decaen et al., 2020), or deep eutectic solvents (Leroy et al., 2012).

Table 3: Tensile mechanical properties of paramylon and curdlan films.

Material	Young's Modulus (MPa)	Stress at break (MPa)	Strain at break (%)
This work 43% (IL:water) plasticized Paramylon (hot pressed at 95°C)	56 ± 9	4.5 ± 0.4	27 ± 3
(Ahmad et al., 2015) 30% Glycerol plasticized curdlan (cast film from solution)	235± 2	9.6 ± 1.3	15 ± 4
(Kawahara & Koganemaru, 2006) Pure paramylon (cast film from solution)	1130	33.9	14.2
(Kawahara et al., 2020) Pure curdlan (hot pressed at 220)C)	1900± 500 Flexural test	60.4 ± 8.2 Flexural test	4.6 ± 0.8 Flexural test

3.5) Recrystallization after processing

During storage at controlled RH, a recrystallization was observed, with the observation of new diffraction peaks at 18.9° (strongest), 24.0°, 28.5°, 29.2° and 30.2° after 30 days (**Figure 1**) for both extruded and hot-pressed samples after 1-month aging. However, DSC analysis of such partially recrystallized films (**Supplementary figures C and D**) did not show significant variations in the endothermic peaks that may be ascribed to melting phenomena: For batch #1, the peak around 45°C is apparently unchanged, while for batch #2, only a slight shift of the maximum of the peak around 75°C towards lower temperatures is observed.

Nevertheless, the decrease of heat flux (i.e. increase of heat capacity) observed on the DSC thermograms below - 20°C appears to be shifted towards higher temperatures for aged samples (**Supplementary figures C and D**). This may be the result of an increase of the glass transition temperature of the amorphous matrix, possibly due to drying.

These new diffraction peaks are also different from those of native paramylon and cannot be indexed in the hexagonal native crystalline lattice. To our knowledge, they were not previously reported for recrystallized paramylon samples, despite Kawahara et al reported a new peak at 18.5° for paramylon samples hot pressed above 200°C (Kawahara et al., 2020). Moreover the recrystallization resulted in the formation of dendrites, visible on photos of aged films (**Figure 5b**) Concurrently, SEM observations of the cross-section of the aged films shows a fibrous structure (**Figure 5e**), with the observation of fibers oriented in the plane of the film (**Figure 5f**). These observations suggest that nanofibers oriented in the plane of the films during processing, may self-associate to form thicker nanofibers during aging. The formation of dendrites may result from a radial orientation of the triple helices or nanofibers in the plane of the film, due to shearing during hot pressing. Future studies may confirm this assumption. Recrystallization is actually a known issue for thermoplastic starches, but strongly depends on the plasticizer used, particularly in the case of ILs (Decaen et al., 2017). Therefore, as for mechanical properties, it would be interesting to investigate the influence of other ionic plasticizers on paramylon recrystallization.

In order to evaluate the reversibility of this recrystallization, some aged films were reprocessed by hot pressing at 95°C, leading to transparent amorphous films again.

4) Conclusions

This work demonstrates that the use of ionic liquids (ILs) as plasticizers can be an alternative to chemical modification in order to achieve thermoplasticity of paramylon. Indeed, the native hexagonal crystalline structure of the biopolymer vanished, just upon mixing with 50% or 43% of a mixture of water and cholinium glycinate (40:60 w:w) (in which paramylon is soluble at 80°C). Only a peak ascribed to the pitch of triple helices was detected by WAXS for this resulting wet powders, in which strong interactions between the polymer and the ionic liquid were evidenced by FTIR. These (paramylon:water:IL) formulations were thermoplastic at 95°C, allowing their melt processing by either extrusion, or hot press, leading to translucent rods and transparent amorphous films, self-reinforced by the triple helices, apparently packed as 10 to 20 nm thick nanofibers. SAXS results suggest that these nanofibers are composed of thinner 4nm nanofibers, as previously observed in native paramylon granules and in self-assembled paramylon nanofibers. However, for the extruded samples this nanostructure is apparently destroyed due to shearing.

For the hot pressed samples, the nanofibers are oriented in the plane of the films, which results in a storage modulus ranging from 300 to 450 MPa at 25°C, depending on the plasticizer content. For the lowest plasticizer content, a ductile tensile behaviour was observed with a strain at break of 27%. For storage times larger than 1 month, a recrystallization of paramylon was observed, with an unidentified crystalline structure different from the native one, and the formation of dendrites. However, these recrystallized samples can be reprocessed into amorphous films by hot pressing at 95°C.

Acknowledgements

The authors would like to thank Nicolas Gautier for TEM observations. This research was funded by CNRS through the MITI interdisciplinary program 80Prime, and by the French National Agency for Research (Agence Nationale de la Recherche, ANR, Grant number ANR-22-CE43-0011-01). A CC-BY public copyright license has been applied by the authors to the present document and will be applied to all subsequent versions up to the Author Accepted Manuscript arising from this submission, in accordance with the grant's open access conditions.

References

Ahmad, M., Nirmal, N. P., & Chuprom, J. (2015). Blend film based on fish gelatine/curdlan for packaging applications: Spectral, microstructural and thermal characteristics. *RSC Advances*, *5*(120), 99044–99057. https://doi.org/10.1039/C5RA20925K

Chen, J., Zeng, X., & Chen, L. (2021). Regulation nature of water-choline amino acid ionic liquid mixtures on the disaggregation behavior of starch. *Carbohydrate Polymers*, *272*, 118474. https://doi.org/10.1016/j.carbpol.2021.118474

Chen, Y., & Wang, F. (2020). Review on the preparation, biological activities and applications of curdlan and its derivatives. *European Polymer Journal*, *141*, 110096. https://doi.org/10.1016/j.eurpolymj.2020.110096

Chuah, C. T., Sarko, A., Deslandes, Y., & Marchessault, R. H. (1983). Packing analysis of carbohydrates and polysaccharides. Part 14. Triple-helical crystalline structure of curdlan and paramylon hydrates. *Macromolecules*, *16*(8), 1375–1382. https://doi.org/10.1021/ma00242a020

Colomines, G., Decaen, P., Lourdin, D., & Leroy, E. (2016). Biofriendly ionic liquids for starch plasticization: A screening approach. *Rsc Advances*, *6*(93), 90331–90337. https://doi.org/10.1039/c6ra16573g

De Santis, S., Masci, G., Casciotta, F., Caminiti, R., Scarpellini, E., Campetella, M., & Gontrani, L. (2015). Cholinium-amino acid based ionic liquids: A new method of

synthesis and physico-chemical characterization. *Physical Chemistry Chemical Physics*, *17*(32), 20687–20698. https://doi.org/10.1039/C5CP01612F

Decaen, P., Rolland-Sabaté, A., Colomines, G., Guilois, S., Lourdin, D., Della Valle, G., & Leroy, E. (2020). Influence of ionic plasticizers on the processing and viscosity of starch melts. *Carbohydrate Polymers*, *230*, 115591. https://doi.org/10.1016/j.carbpol.2019.115591

Decaen, P., Rolland-Sabate, A., Guilois, S., Jury, V., Allanic, N., Colomines, G., Lourdin, D., & Leroy, E. (2017). Choline chloride vs choline ionic liquids for starch thermoplasticization. *Carbohydrate Polymers*, *177*, 424–432. https://doi.org/10.1016/j.carbpol.2017.09.012

Feuzing, F., Mbakidi, J. P., Marchal, L., Bouquillon, S., & Leroy, E. (2022). A review of paramylon processing routes from microalga biomass to non-derivatized and chemically modified products. *Carbohydrate Polymers*, *288*, 119181. https://doi.org/10.1016/j.carbpol.2022.119181

Futatsuyama, H., Yui, T., & Ogawa, K. (1999). Viscometry of Curdlan, a Linear (1→3)-β- D -Glucan, in DMSO or Alkaline Solutions. *Bioscience, Biotechnology, and Biochemistry*, *63*(8), Article 8. https://doi.org/10.1271/bbb.63.1481

Gan, H., Enomoto, Y., Kabe, T., Ishii, D., Hikima, T., Takata, M., & Iwata, T. (2017). Synthesis, properties and molecular conformation of paramylon ester derivatives. *Polymer Degradation and Stability*, *145*, 142–149. https://doi.org/10.1016/j.polymdegradstab.2017.05.011

Hopson, C., Villar-Chavero, M. M., Domínguez, J. C., Alonso, M. V., Oliet, M., & Rodriguez, F. (2021). Cellulose ionogels, a perspective of the last decade: A review. *Carbohydrate Polymers*, *274*, 118663. https://doi.org/10.1016/j.carbpol.2021.118663

Kawahara, Y., & Koganemaru, A. (2006). Development of novel film using paramylon prepared fromEuglena gracilis. *Journal of Applied Polymer Science*, *102*(4), Article 4. https://doi.org/10.1002/app.24618

Kawahara, Y., Ohtani, T., & Nakamura, M. (2020). Direct Resinification of Two (1→3)-β-D-Glucans, Curdlan and Paramylon, via Hot-Press Compression Molding. *Publication Cover Journal of Macromolecular Science, Part B*, 635–647.

Kiss, J. Z., Vasconcelos, A. C., & Triemer, R. E. (1987). STRUCTURE OF THE EUGLENOID STORAGE CARBOHYDRATE, PARAMYLON. *American Journal of Botany*, *74*(6), 877–882. https://doi.org/10.1002/j.1537-2197.1987.tb08691.x

Kobayashi, K., Kimura, S., Togawa, E., Wada, M., & Kuga, S. (2010). Crystal transition of paramylon with dehydration and hydration. *Carbohydrate Polymers*, *80*(2), Article 2. https://doi.org/10.1016/j.carbpol.2009.12.009

Kono, H., Kondo, N., Isono, T., Ogata, M., & Hirabayashi, K. (2020). Characterization of the secondary structure and order–disorder transition of a β-(1 → 3, 1 → 6)-glucan from Aureobasidium pullulans. *International Journal of Biological Macromolecules*, *154*, 1382–1391. https://doi.org/10.1016/j.ijbiomac.2019.11.018

Leroy, E., Decaen, P., Jacquet, P., Coativy, G., Pontoire, B., Reguerre, A. L., & Lourdin, D. (2012). Deep eutectic solvents as functional additives for starch based plastics. *Green Chemistry*, *14*(11), 3063–3066. https://doi.org/10.1039/c2gc36107h

Mangolim, C. S., da Silva, T. T., Fenelon, V. C., do Nascimento, A., Sato, F., & Matioli, G. (2017). Use of FT-IR, FT-Raman and thermal analysis to evaluate the gel formation of curdlan produced by Agrobacterium sp. IFO 13140 and determination of its rheological properties with food applicability. *Food Chemistry*, *232*, 369–378. https://doi.org/10.1016/j.foodchem.2017.04.031

Marchessault, R. H., & Deslandes, Y. (1979). Fine structure of (1→3)-β-d-glucans: Curdlan and paramylon. *Carbohydrate Research*, 231–242.

Mateyawa, S., Xie, D. F., Truss, R. W., Halley, P. J., Nicholson, T. M., Shamshina, J. L., Rogers, R. D., Boehm, M. W., & McNally, T. (2013). Effect of the ionic liquid 1-ethyl-3-methylimidazolium acetate on the phase transition of starch: Dissolution or gelatinization? *Carbohydrate Polymers*, *94*(1), 520–530. https://doi.org/10.1016/j.carbpol.2013.01.024

Noble, A., Swain, A., Clarke, Charles, Jonathan, Zhang, Chonggang, Sabouri, Shomayeh, Li, Shaojin, Long, Adam, William, & Sasidharan Pilai, Prasanth Kumar. (2020). *Compositions, preparation and uses of paramylon* (Patent No. WO 2020/178718 A1).

Sankri, A., Arhaliass, A., Dez, I., Gaumont, A. C., Grohens, Y., Lourdin, D., Pillin, I., Rolland-Sabate, A., & Leroy, E. (2010). Thermoplastic starch plasticized by an ionic liquid. *Carbohydrate Polymers*, *82*(2), 256–263. https://doi.org/10.1016/j.carbpol.2010.04.032

Sciarini, L. S., Rolland-Sabate, A., Guilois, S., Decaen, P., Leroy, E., & Le Bail, P. (2015). Understanding the destructuration of starch in water-ionic liquid mixtures. *Green Chemistry*, *17*(1), 291–299. https://doi.org/10.1039/c4gc01248h

Shibakami, M. (2017). Thickening and water-absorbing agent made from euglenoid polysaccharide. *Carbohydrate Polymers*, *173*, 451–464. https://doi.org/10.1016/j.carbpol.2017.06.025

Shibakami, M., Nemoto, T., & Sohma, M. (2018). Dependence of dissolution, dispersion, and aggregation characteristics of cationic polysaccharides made from euglenoid β-1,3-glucan on degree of substitution. *Cellulose*, *25*(4), Article 4. https://doi.org/10.1007/s10570-018-1740-4

Shibakami, M., & Sohma, M. (2017). Synthesis and thermal properties of paramylon mixed esters and optical, mechanical, and crystal properties of their hot-pressed films. *Carbohydrate Polymers*, *155*, 416–424. https://doi.org/10.1016/j.carbpol.2016.08.093

Shibakami, M., & Sohma, M. (2018). Thermal, crystalline, and pressure-sensitive adhesive properties of paramylon monoesters derived from an euglenoid polysaccharide. *Carbohydrate Polymers*, *200*, 239–247. https://doi.org/10.1016/j.carbpol.2018.08.005

Shibakami, M., Tsubouchi, G., & Hayashi, M. (2014). Thermoplasticization of euglenoid β-1,3-glucans by mixed esterification. *Carbohydrate Polymers*, *105*, 90–96. https://doi.org/10.1016/j.carbpol.2014.01.053

Shibakami, M., Tsubouchi, G., Nakamura, M., & Hayashi, M. (2013). Polysaccharide nanofiber made from euglenoid alga. *Carbohydrate Polymers*, *93*(2), 499–505. https://doi.org/10.1016/j.carbpol.2012.12.040

Tao, D.-J., Cheng, Z., Chen, F.-F., Li, Z.-M., Hu, N., & Chen, X.-S. (2013). Synthesis and Thermophysical Properties of Biocompatible Cholinium-Based Amino Acid Ionic Liquids. *Journal of Chemical & Engineering Data*, *58*(6), 1542–1548. https://doi.org/10.1021/je301103d

Xie, F. W., Flanagan, B. M., Li, M., Sangwan, P., Truss, R. W., Halley, P. J., Strounina, E. V., Whittaker, A. K., Gidley, M. J., Dean, K. M., Shamshina, J. L., Rogers, R. D., & McNally, T. (2014). Characteristics of starch-based films plasticised by glycerol and by the ionic liquid 1-ethyl-3-methylimidazolium acetate: A comparative study. *Carbohydrate Polymers*, *111*, 841–848. https://doi.org/10.1016/j.carbpol.2014.05.058

Yasuda, K., Ogushi, M., Nakashima, A., Nakano, Y., & Suzuki, K. (2018). Accelerated Wound Healing on the Skin Using a Film Dressing with β-Glucan Paramylon. *In Vivo*, *32*(4), 799–805. https://doi.org/10.21873/invivo.11310

Zhang, B., Xie, F., Shamshina, J. L., Rogers, R. D., McNally, T., Wang, D. K., Halley, P. J., Truss, R. W., Zhao, S., & Chen, L. (2017). Facile Preparation of Starch-Based Electroconductive Films with Ionic Liquid. *ACS Sustainable Chemistry & Engineering*, *5*(6), 5457–5467. https://doi.org/10.1021/acssuschemeng.7b00788